PROTEINS: Structure, Function, and Genetics 39:317–330 (2000)

Electrostatic Properties of Bovine β-Lactoglobulin

Federico Fogolari,[1]* Laura Ragona,[2] Stefania Licciardi,[1] Silvia Romagnoli,[1] Roberta Michelutti,[1] Raffaella Ugolini,[1] and Henriette Molinari[1,2]

[1]*Dipartimento Scientifico e Tecnologico, Università di Verona, Verona, Italy*
[2]*Laboratorio NMR, CNR, Milano, Italy*

ABSTRACT **Bovine β-Lactoglobulin (BLG) has been studied for many decades, but only recently structural data have been obtained, making it possible to simulate its molecular properties. In the present study, electrostatic properties of BLG are investigated theoretically using Poisson-Boltzmann calculations and experimentally following pH titration via NMR. Electrostatic properties are determined for several structural models, including an ensemble of NMR structures obtained at low pH. The changes in electrostatic forces upon changes in ionic strength, solvent dielectric constant, and pH are calculated and compared with experiments. pK_as are computed for all titratable sites and compared with NMR titration data. The analysis of theoretical and experimental results suggests that (1) there may be more than one binding sites for negatively charged ligands; (2) at low pH the core of the molecule is more compact than observed in the structures obtained via restrained molecular dynamics from NMR data, but loop and terminal regions must be disordered. Proteins 2000; 39:317–330.** © 2000 Wiley-Liss, Inc.

Key words: Poisson-Boltzmann; continuum methods; electrostatic forces; protein titration; NMR

INTRODUCTION

Bovine β-Lactoglobulin (BLG) is a 18 kDa widely studied protein belonging to the Lipocalin superfamily of transporter molecules for small hydrophobic ligands. Its structural characterization has been reported by X-ray[1–3] and NMR.[4–8] Diffraction studies were performed at physiological pH, where the protein is a dimer of about 36 kDa molecular weight, consisting of nine anti-parallel β-strands and one terminal α-helix segment. NMR characterization was instead obtained at acidic pH, where β-LG is a monomer adopting a β-barrel fold similar to that observed at neutral pH, characterized by the presence of disordered loops and terminal regions. The β-sheet segments of β-LG form a calyx structure with a hydrophobic buried cluster conferring stability to the protein while a hydrophobic surface patch, localized in a groove between the strands and the helix, provides stabilising hydrophobic interactions between the barrel and the flanking terminal helix.[5]

In spite of the fact that BLG is known to bind several nonpolar ligands such as retinol, fatty acids, protoporphyrin IX, cholesterol, estradiol, and progesterone,[9] its biological function is still unclear. However, as a consequence of its binding properties and its high structural homology with retinol and fatty acid binding proteins, it has been proposed that it may have a transport role for these ligands. Perez et al.[10] have suggested that ruminant BLG, because of its capacity to bind fatty acids, might play a role in the activity of pre-gastric lipase. This lipase participates in fat digestion in the stomach and is important in the neonatal period, because the levels of pancreatic lipase and bile salts are low at this age. Furthermore, pre-gastric lipase is unique among the digestive tract lipases in its ability to attack the native milk fat globule, leading to increases in its subsequent hydrolysis by pancreatic lipase. It is remarkable that BLG enhances the activity of this lipase at the concentrations found in milk and during the colostral period. This effect is probably due to the removal of free fatty acids, which inhibit the enzyme. These facts indicate that the biological role of BLG in ruminants could be to participate in milk fat digestion in the newborn, promoting pregastric lipase activity.

The molecular mechanism of ligand binding and release is poorly understood and a detailed study of the electrostatic properties of this protein, reported here, could help in understanding its stability and behaviour towards association and binding.

The influence pH exerts on protein structure is widely believed to be electrostatic in nature via changes in the protonation state of titratable groups, which in turn influence processes like ligand uptake or release, partial or global unfolding, and protein-protein association.

We have used NMR and molecular modelling to elucidate BLG (genetic variant B) (Scheme 1) structure and dynamics at low pH[4–6,8] and we report here a thorough study on electrostatics for different conformational models of BLG. In particular we consider (1) the dimer structure determined by Brownlow and co-workers at pH 6.5 via X-ray crystallography[1]; (2) the two monomers artificially excised from the dimer; (3) a new ensemble of structures for the monomer at low pH obtained from published and additional NMR data.[6]

For all these models we calculate: the apparent pK_a for all titratable sites, the protonation state of the protein at different pH's, and the electrostatic potential at the solvent accessible surface which may suggest binding sites for charged or polar ligands. Additionally, we have com-

Grant sponsor: Italian MURST.

*Correspondence to: Federico Fogolari, Dipartimento Scientifico e Tecnologico, Universita di Verona, Cà Vignal 1, Strada Le Grazie, 37134 Verona, Italy. E-mail: fogolari@sci.univr.it

Received 5 November 1999; Accepted 28 January 2000

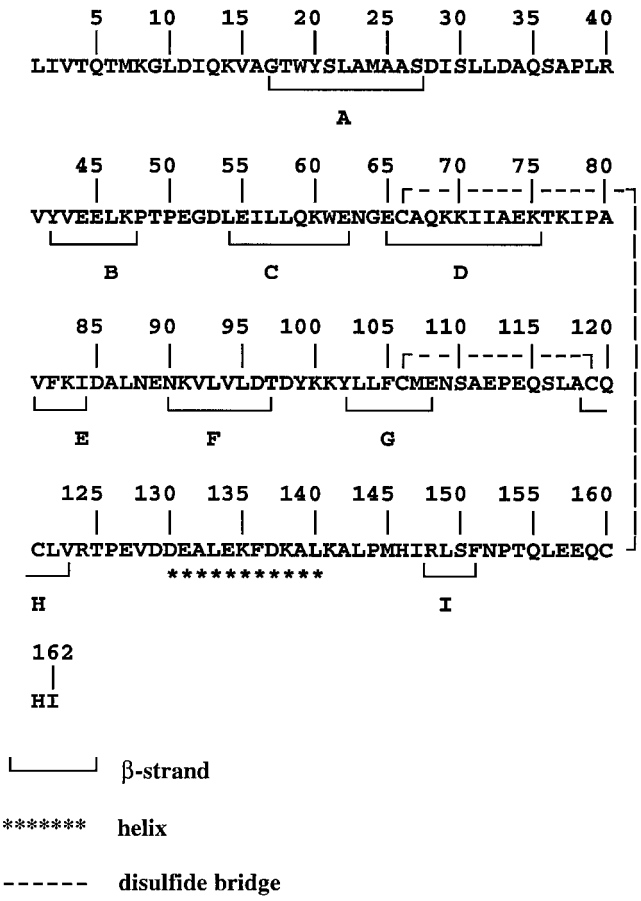

Scheme 1. BLG primary and secondary structure.

puted the apparent pK_a and the protonation state of the protein for the recently deposited monomeric structures in the Protein Data Bank for the variant B structure obtained at pH 7.1[3] and the complex β-LG-palmitate[11] with palmitate excised from the structure to probe the effect of the opening of the EF loop. We titrate the protein at low pH via NMR, and the comparison of theoretical data and our and literature experimental data support the overall validity of the NMR derived models. We believe our results provide a rationale for experimental observations and suggest some functional implication.

THEORETICAL BACKGROUND

Poisson-Boltzmann Equation

The theory of electrostatic interactions in biomolecules has a long history and has been thoroughly reviewed in several papers[12-14] and will not be repeated here in detail. We summarize here only the main features of the methodology we follow. The key approximation, which has proven both practical and useful, treats the protein as a fixed low dielectric cavity and the solvent as a high dielectric continuum medium. The approximation finds its rationale in the largely different time scales on which solute and solvent motions take place, so that for each biomolecular conformation solvent effects are effectively averaged.[15]

The electrostatic potential for this model system obeys the Poisson equation (commonly reported in in c.g.s.units):

$$\nabla \cdot [\varepsilon(r)\nabla\psi(r)] + 4\pi\rho(r) = 0 \quad (1)$$

where $\psi(r)$ is the average electrostatic potential, $\epsilon(r)$ is the dielectric constant, and $\rho(r)$ is the charge density. Salts may be also included in a self-consistent way into this scheme with the additional assumption that the potential of mean force for an ion of valency z is $zq\psi(r)$ where q is the protonic charge.

Finally a second order differential equation for the average electrostatic potential (the Poisson-Boltzmann [PB] equation) is obtained

$$\bar{\nabla} \cdot [\varepsilon(r)\bar{\nabla}\psi(r)] = -4\pi\rho^f(r) - 4\pi \sum_i c_i^\infty z_i q \exp\left(\frac{-z_i q\psi(r)}{kT}\right) \quad (2)$$

where $\rho^f(r)$ includes only molecular charges, c_i^∞ is the concentration of ion i at an infinite distance from the molecule, z_i is its valency, q is the proton charge, k is the Boltzmann constant and T is the temperature.

The equation may be further simplified by linearizing the exponential. This appears to be a satisfactory approximation for most purposes.[16]

Numerical Solution of the PB Equation

Except for a few systems possessing simple geometry, the PB equation must be solved numerically. Common methods to solve the PB equation include boundary elements techniques (for which inclusion of salts is not straightforward) and the finite differences method. In the latter approach, the dielectric map, the atomic point charges of the solute, and the salt accessibility map are discretized onto a grid. The Poisson-Boltzmann equation is converted in a set of finite difference equations (one for each point of the grid), which is solved via an iterative procedure.[14,17,18] The result is the electrostatic potential on each point of the grid. One common problem implicit in the discretization procedure is that the electrostatic potential at nodes inside the molecule is strongly dependent on the grid position and mesh, so that, in order to compare different states of a molecule these unwanted effects must be cancelled out in comparison.[14,19]

Electrostatic Potential at Solvent Accessible Surface

A direct and common use of the solution of the PB equation is the visualization of the electrostatic potential at the solvent accessible surface of the molecule. Complementary electrostatic properties at interacting surfaces have been observed for biomolecular complexes.[13,20] Moreover, the electrostatic potential at the surface is directly related to the Boltzmann space distribution at the surface of small electrolytes or polar molecules, in the commonly adopted assumption that the small molecule does not influence significantly the electrostatic potential due to the macromolecule. Visual inspection of the electrostatic potential at the surface may suggest preferential binding sites for charged ligands or groups in a ligand. Obviously, the values obtained should be regarded only in a semiquantita-

tive manner, since the continuum approximation is worse closer to the biomolecular surface where averaging of solvent effects is hindered by the macromolecule.

Electrostatic Free Energies

The electrostatic potential may be also employed to compute the electrostatic free energy for the hypothetical process of charging the solute in an ionic atmosphere. Rather than in the absolute values of the free energy, one is usually interested in the comparison of different states of the molecules, e.g., in varying salt concentrations or association states.

The functional form for the free energy has been a matter of debate in the field of colloid chemistry (for a review see Verwey and Overbeek[21]), but may be consistently derived from standard thermodynamics considerations[22,23] or (with some caution) from a variational principle.[24,25]

The electrostatic free energy of the system (ΔG^{es}) is composed by a classical electrostatic term of the form charge times potential (ΔG^{cp}), a term describing the entropy of mixing of the ions (ΔG^{mix}) and a term due to the solvent (ΔG^{solv}), i.e., the so-called osmotic term, where the different terms read:

$$\Delta G^{es} = \Delta G^{cp} + \Delta G^{mix} + \Delta G^{solv} \tag{3}$$

$$\Delta G^{cp} = \int_v \frac{\rho\psi}{2}\,\mathrm{d}V \tag{3a}$$

$$\Delta G^{mix} = kT \int_v \sum_i c_i \ln \frac{c_i}{c_i^{\infty}}\,\mathrm{d}V \tag{3b}$$

$$\Delta G^{solv} = kT \int_V \sum_i c_i^{\infty}\left[1 - \exp\left(\frac{-z_i q\psi}{kT}\right)\right]\mathrm{d}V \tag{3c}$$

It should be noted that, due to the temperature dependence of the dielectric constant, the entropy terms of the free energy are not coincident with ΔG^{mix} and ΔG^{solv}, but must be computed from the temperature dependence of the free energy.[26,27]

If the linear approximation holds the only term contributing the free energy is ΔG^{cp} where the charge density includes the charges on the biomolecule, but not salt charges. Moreover, a consequence of the linearization is that the superposition principle applies and therefore the electrostatic free energy may be expressed as:

$$\Delta G^{cp} = \frac{1}{2}\sum_{ij} q_i q_j \phi_{ij} \tag{3d}$$

where ϕ_{ij} are the values the Green's function $\phi(\vec{r}_1, \vec{r}_2)$ takes on sites i and j.

Electrostatic Forces

Electrostatic forces are obtained in the present approach as derivatives of the free energy in its linear form.[28] Electrostatic free energies are computed from the following equation:

$$\Delta G^{el} = \sum_{i>j} \frac{q_i q_j}{\varepsilon r_{ij}} + \Delta G^{solv,el} \tag{4}$$

where $\Delta G^{solv,el}$ is the electrostatic contribution to the energy for transferring the molecule from a phase possessing its inner dielectric constant to solution, conveniently computed by UHBD. Electrostatic forces entail three terms:

$$\vec{F}_i^{\,el} = q_i \vec{E}_i - \frac{1}{8\pi}|\vec{E}|^2 \nabla_i \varepsilon - \frac{1}{8\pi}\varepsilon k_D^2 \nabla_i \lambda \tag{5}$$

where $\vec{E}$ is the electric field at atom i and λ is the solvent accessibility. In this equation the second and third term represent electrostatic and ionic pressure. In all calculations ionic pressure, which is expected to be much smaller than other contributions, is neglected.[28]

Protein Titration

The difference in the free energy cost of protonation (or deprotonation) of a titratable group in a model compound and in a biomolecule, ΔG, implies a shift in its pK_a according to the equation: $\Delta pK_a = \Delta G/2.303RT$, and therefore the protonation state of a titratable group may differ in different molecular environments. For the modelization of multiple titratable sites we follow closely the approach of Bashford and Karplus[29] as modified by Antosiewicz et al.[30] and consider the ionization process by adding a positive or a negative charge on a single atom in the titratable group. We can consider the ensemble of ionization states of the molecule as a set of charges $\{z_i\}$, where the index i runs on all atoms, which assume the value 0 for most atoms, and the values 0 or ±1 proton charge for the selected atom in each titratable group, according to its protonation state.

The free energy of ionization, with respect to the molecule with all ionizable sites uncharged may be expressed, within the linear approximation for the Poisson-Boltzmann equation, as:

$$\Delta G = \left(\frac{1}{2}\sum_{ij}((q_i + z_i)(q_j + z_j)\phi_{ij}^N) - \frac{1}{2}\sum_{ij}(q_j q_i \phi_{ij}^N)\right) - \left(\frac{1}{2}\sum_{ij}((q_i + z_i)(q_j + z_j)\phi_{ij}^M) - \frac{1}{2}\sum_{ij}(q_j q_i \phi_{ij}^M)\right) + \sum_i 2.303RTz_i(pK_a^{i,M} - pH) \tag{6}$$

where indices i and j run on all atoms and superscript M and N refer to a model compound for which pK_as are known, and to the biomolecule, respectively. The reference pK_as are usually measured on small peptides containing the aminoacid of interest. In order to cancel self-energy terms, a good model for these small peptide compounds are the isolated (i.e., non-interacting) aminoacids artificially excised from the molecule, assuming that the pK_a for these hypothetical compounds would be the same as that measured on small peptides. Under this assumption, equation (6) further simplifies:

$$\Delta G = \frac{1}{2}\sum_i z_i^2(\phi_{ii}^N - \phi_{ii}^M) + \left(\sum_{ij}^{N}(z_i q_j \phi_{ij}^N) - \sum_{ij}^{M}(z_i q_j \phi_{ij}^M)\right) + \sum_{i>j}(z_i z_j \phi_{ij}^N) + \sum_i z_i 2.303RT(pH - pK_a^{i,M}) \quad (7)$$

Here the Green's function between atoms belonging to different aminoacids in the model compound is zero (i.e., $\phi_{ij}^M = 0$ if i and j refer to atoms in different residues). The first term in this equation represents the difference in self-energy upon placing a charge z_i in the titratable site in the protein and in the model compound, the second term is the so-called background term due to the interaction between the charge z_i and the other partial charges (when all other ionizable groups are uncharged) in the protein and in the model compound, the third term represents the interaction between titratable sites in the protein, and the fourth term is the free energy of ionization at a given pH for the model compound.

The free energy equation (7) can be used to generate the statistical charge state of each ionizable site at each pH using a Monte Carlo method.[31]

MATERIALS AND METHODS

Surface Electrostatic Potential Calculation

All electrostatics calculations were performed using the software package UHBD,[32] which solves the Poisson-Boltzmann equation using the finite difference method.

Partial atomic charges and van der Waals radii were assigned using the CHARMM forcefield.[33,34] Electrostatic maps were obtained using initially a coarse grid of 60×60×60 spaced 2.5 Å, and then focusing on the molecule using a grid of 110×110×110 points with a mesh of 0.8 Å. A standard choice for relevant parameters was adopted, i.e., 1.4 Å for surfacing probe radius, 2 Å for ionic exclusion radius, 100 mM for ionic strength, 4 and 80 for protein and solvent dielectric constants, respectively. The potential at the boundary for the initial grid was set to zero, and then the boundary conditions were obtained interpolating from the coarse grid. Maps were converted into 65×65×65 points map and visualized using the software package GRASP.[35]

Some care must also be taken in order to avoid effects due to poor definition of the solvent accessible surface, which is difficult to avoid with a mesh which is often comparable to surfacing probe radius. In going from the inner of the solute to the solvent the potential may change by one order of magnitude. For this reason, we have used a surfacing probe radius of 2 Å for visualization so that the visualized potential should refer in any case to the solvent.

Electrostatic Forces Calculation

All electrostatic forces calculations were performed using the software package UHBD.[32] Electrostatic forces on each atom were obtained starting from a grid of 110×110×110 points spaced 2.0 Å centered on the molecular center of geometry, and then focusing with a grid of 110×110×110 points spaced 1.0 Å and finally focusing on each aminoacid with a grid of 30×30×30 points spaced 0.4 Å. Electrostatic forces acting on each atom and the resultant of the forces acting on each aminoacid were examined. Most molecular analysis to detect contacting residues have been performed using the program WHATIF.[36]

Theoretical Protein Titration

We compute first with two single finite difference calculations the Green's function and the background term for each titratable site in the protein and in the isolated amino acid. Then, we use a Monte Carlo procedure, employing 100,000 steps with a single charge variation, to generate, at different pH's ranging from −2.0 to 16.0 (for fitting purposes) in steps of 0.5 units, a statistical ensemble of ionization states[30] and calculate ensemble averages. The average protonation state $\langle q \rangle$ vs. pH is then fitted using the single site equation:

$$\langle q \rangle = \frac{\exp[2.303RT(pK - pH)]}{1 + \exp[2.303RT(pK - pH)]} \quad (8)$$

using pK as the fitting parameter.

Following Antosiewicz et al.[30] (see references cited therein) the reference pK_a for the isolated amino acid (pK_a^M) was 7.5 for the N-terminal amino group (atom N according to PDB nomenclature was the titratable site), 12.0 for the guanidinium group of arginine (atom CZ), 10.4 for the amino group in lysine (atom NZ), 6.3 for the imidazole group (atom ND1), 3.8 for the C-terminal carboxyl group (atom C), 4.0 for the aspartic carboxyl group (atom CG), 4.4 for the glutamic carboxyl group (atom CD), 8.3 for the thiol group in free cysteine (atom SG), and 9.6 for the phenol group in tyrosine (atom OH). Except for Tyrosines and Cysteine, for all other titratable groups we have chosen the ionized form of the aminoacid for the dielectric map generation and partial charges were slightly changed, with respect to the original parameters, accordingly. Hydrogens were added to the crystallographic structures using the program InsightII (MSI, San Diego, CA). Histidines were not involved in possible salt bridges and, therefore, no particular choice was adopted concerning the protonation model although improvements to this scheme have been described by Demchuck and Wade.[37]

We have computed the titration curve for all molecular models mentioned in the theory section, using charge and radii parameters from the united atom set from Antosiewicz et al.[30] and from the all atom parameter set CHARMM.[33,34] First a grid of 40×40×40 points spaced by 2.5 Å was computed and then three focusing steps employing grids of 15×15×15 points spaced 1.2 and 0.75 Å and finally a grid of 20×20×20 points spaced 0.25 Å. The dependence of the results on the grid size is negligible whereas there are sizeable differences due to the set of parameters used. We report here only results obtained using the set of parameters PKAS since the methodology has been extensively tested on these parameters.[30]

NMR Structure Determination

An ensemble of ten structures was determined essentially as previously described.[6] Compared to the previous work, we slightly modified the standard Dyana simulated annealing procedure in order to obtain better Ramachandran plots for the structures. Disallowed conformations in a

Fig. 1. Stereoview of the ensemble of ten NMR structures superimposed on the chain A (shown as a ribbon) of the X-ray structure of BLG (PDB id.:1beb). Only residues corresponding to secondary structure elements are shown (i.e., residues 17–26, 42–48, 54–62, 65–75, 81–84, 90–97, 102–108, 118–123, 130–140, 148–151).

large number of loop and terminal residues result from combination of lack of restraints and soft repulsive cores. We have restrained all backbone ϕ angles in the range -180 to 0°, except at glycines, and at those residues for which evidence for positive ϕ values had been found in the X-ray structure[1] (i.e., Ala 34, Leu 39, Leu 87, Asn 88, Tyr 99, Asn 159, and Cys 160). The rationale behind this choice was that additional unfavorable ϕ values (compared to the crystal structure) would hardly be adopted in a less restrained and overall similar structure as the one in solution at low pH.

pH Titration

The effect of pH titration on the chemical shifts of protons was determined by analyzing a series of TOCSY spectra recorded at eight different pH values ranging from 1.3 to 3.3. At pH values higher than 3.3 the aggregation of the protein leads to severe broadening, thus preventing the analysis of the spectra. Chemical shifts of protons were referenced to the frequency of TSP dissolved in the buffer solution at pH 2.0 using an internal capillary. Minor adjustements were performed on the reference frequency for better matching of the spectra.

The measurements were performed at pH 1.3, 1.6, 1.8, 2.1, 2.4, 2.6, 3.1, and 3.3, at room temperature. The pH was checked before and after each NMR experiment. For most resonances, the chemical shift differences between consecutive spectra were small and allowed an easy assignment by comparison with the assigned spectra under the reference conditions.[4,6] All two-dimensional spectra were analysed on a SGI Indigo2 workstation using the program XWINNMR (Bruker Instruments Inc.) and XEASY.[38]

pK_as values were determined by measuring the changes in the ^{1}H resonance of selected residues, free from overlap, as a function of pH. pK_a values and the chemical shift limiting values at low and high pH were calculated by a non-linear least-squares fit of the experimental pH titration curve to the following equation

$$\delta_{obs} = \frac{\delta_l + \delta_h \times 10^{(pH - pKa)}}{1 + 10^{(pH - pKa)}} \qquad (9)$$

where subscript *obs*, refer to the observed chemical shift at the given pH, and subscripts l and h refer to the chemical shift limiting value at low and high pH, respectively.

Only resonances assigned under most experimental conditions were used for the analysis; resonances displaying small chemical shifts changes (typically less than 0.07 ppm) were regarded as pH independent.

RESULTS AND DISCUSSION

NMR Structure Determination

The almost complete assignment of the ^{1}H spectrum recently obtained using heteronuclear NMR by Barlow and coworkers[7] allowed us to identify and assign some additional through space connectivities in the NOESY spectra with respect to those previously reported and therefore to obtain a larger number of restraints. The total number of integrated NOE's was as follows: 237 intraresidue, 175 sequential, 57 medium range and 193 long range, which led to 122 intraresidue, 171 sequential, 59 medium range and 217 long range nonredundant restraints. As a consequence of the additional restraints, the overall definition of the structure has improved (Fig. 1).

The average pairwise RMSD between the structures in the ensemble is 1.93 ± 0.47 , when backbone atoms of amino acids 17–26, 42–48, 54–62, 65–75, 81–84, 90–97, 102–108, 118–123, 130–140, 148–151, corresponding to well defined secondary structural elements are superimposed. When backbone atoms of residues 15–26, 42–49, 53–59, 70–71, 73–75, 80–83, 91–97, 101–108, 117–125, 131–140, which display a RMSD less than 2.0 Å, are superimposed their RMSD is 1.27 ± 0.21 Å.

The average RMSD of the NMR structures with the X-ray structures, superimposing only the backbone atoms of the residues emcompassing strands A to H, is 1.90 ± 0.39 Å for monomers A and B deposited by Brownlow and coworkers[1] (PDB id.: 1beb), 1.92 ± 0.41 Å for the structure deposited by Jameson and coworkers[3] determined at pH 7.1 (PDB id.: 1bsq), 1.97 ± 0.37 Å for the structure complexed with palmitate (PDB id.: 1b0o).[11]

With respect to our previous report the terminal helix is better defined and closer to the X-ray structures, while strand I and the loop connecting strands C and D and flanking residues still appear to be loosely defined. As before, it is difficult to assess whether the lack of definition is due to poor restraints or real mobility. H-D exchange data provide a quantitative answer to this question.[8]

Electrostatic Properties at Solvent Accessible Surfaces

We have calculated electrostatic potential maps at neutral and acidic pH. For neutral pH we considered the dimer

structure deposited in the PDB (id.: 1beb)[1], with few amino acids whose electron density was missing in the original data added manually using InsightII (MSI/Biosym, San Diego, CA). The structure was obtained from crystals containing a mixture of A and B variants, and the deposited structure has a valine at position 118 (like in variant A) and a glycine at position 64 (like in variant B). We replaced Val 118 with Ala 118 to obtain a structure corresponding to a pure genetic variant B. Such replacement is not expected to lead to any significant structural change[3].

At neutral pH, all carboxyl groups have been assumed to be deprotonated and all basic residues (including histidines) to be protonated, while at acidic pH all residues were assumed to be protonated. At low pH, we examined both monomers artificially excised from the dimer and the ten NMR structures. In order to check for the dependence of the results on loops and poorly defined regions, we computed maps for the isolated monomers from the X-ray structure with residues 1–13, 27–41, and 143–162, cancelled from the coordinate file. For all molecular models, we sorted surface positions by their electrostatic potential values and examined all points showing the highest or lowest potential. The threshold potential values were chosen different from map to map in order to retain only points that corresponded to the highest potential spots found by visual inspection (1.5 kcal/mol · q and −2.0 kcal/mol · q for the highest and lowest potential surface points for maps at neutral pH, and close to 2.5 kcal/mol · q for maps at pH 2.0 in order to retain only the highest 200 points). The points chosen were seen to cluster around well-defined positions. For each cluster of points, all residues that had at least one atom within 4 Å were marked in order to localize the high potential spots. This analysis confirmed and further detailed the previously reported one.[6]

For the dimer at neutral pH (PDB id. 1beb), there are two large and two less extended high potential surface regions:

The larger one is close to atoms belonging mainly to residues in the loop DE and on strands E and F and is found on both chains (i.e., residues 76, 78, 81–83, 90–91, 110 on chain A and 76–78, 90–91, 110 on chain B);

The other large area is located at the open end of the calyx (i.e., at residues 60, 62, 69, 87 on chain A).

The two minor regions are located at the interface between the FG loop and the terminal α-helix and at the end of the same helix (100, 101, 138, 141 on chain A).

The latter regions are among the highest potential ones only on chain A due to different sidechain orientations (namely sidechains of residues Lys 60, Glu 74, Lys 77, Lys 83, Lys 101, Glu 131 and Lys 141). A large number of low (less than −2 kcal/mol · q) electrostatic potential surface points are found as well all over the solvent accessible surface at neutral pH.

All four regions are, however, found as highest potential regions (involving also additional residues) at pH 2 on both isolated monomers with or without flexible regions (shown in Fig. 2 on chain A). In particular, the open end of the calyx and the helix/FG loop interface are the regions of most extended high surface potential. We have found a similar behaviour, with some degree of variability, on the ensemble of NMR structures.

Implications for Binding

The main effects high electrostatic surface potential (usually associated with high electric fields) may exert on binding are related: (1) to the direct electrostatic interaction between the molecule and charged or polar ligands at the surface, and (2) to the steering effect on their diffusional encounter. This picture would be consistent with the positioning of the charged head of both 12-bromododecanoic[39] and palmitic acid[11] at the open end of the calyx. A consequence of this model would also be that since the charged head is driven, during molecular encounter, toward the open end of the calyx, the entrance of the aliphatic chain inside the calyx would require partial opening of the strands entailing the barrel. The recent NMR analysis of hydrogen/deuterium exchange for all structural elements of BLG[8] pointed out that, besides flexible regions, the highest number of fast exchanging residues is found in strand D and in the N-terminal region of the α-helix, as expected from helix hydrogen bonding pattern. It is difficult to establish whether such conclusions concerning stability hold at higher pH, where NMR measurements are hindered by dimerization. If this would be the case, the shortest DE interface would be a candidate for letting the aliphatic fatty acid chain inside the barrel. A similar "portal area" has been proposed recently for bovine heart fatty acid binding protein.[40] At low pH, the picture is different because the carboxylic head of palmitic acid is protonated and favorable electrostatic interactions with the protein are disrupted and binding does not take place (Ragona et al., unpublished data).

It should be noted that the high potential region at the helix/FG loop region is close to a hydrophobic cluster which has been suggested as possible binding site for hydrophobic ligands.[5] In view of the present considerations, both hydrophobic and electrostatically driven binding should be considered when interpreting experimental data. Somewhat puzzling binding results, with a stoichiometry ranging from one ligand per dimer for palmitic acid[41] to three ligands per monomer for ANS,[42] could simply reflect the different mechanisms of binding. For ANS, which is likely to bear a negative unit charge even at pH 2.5, both hydrophobic and electrostatic binding can be anticipated explaining the high stoichiometry observed. For other compounds, it can be anticipated that the high potential surface regions (including the calyx open end and the helix-barrel interface) can better accomodate negatively charged or polar moieties.

Electrostatic Forces

Another important electrostatic effect is related to electrostatic forces.[28] In this respect, it is significant that large changes in chemical shifts upon mild salt and urea additions have been observed for residues corresponding to the low pH high potential regions located at the terminal α-helix and FG loop.[6] An explicit calculation of the change in total electrostatic forces acting on each residue upon

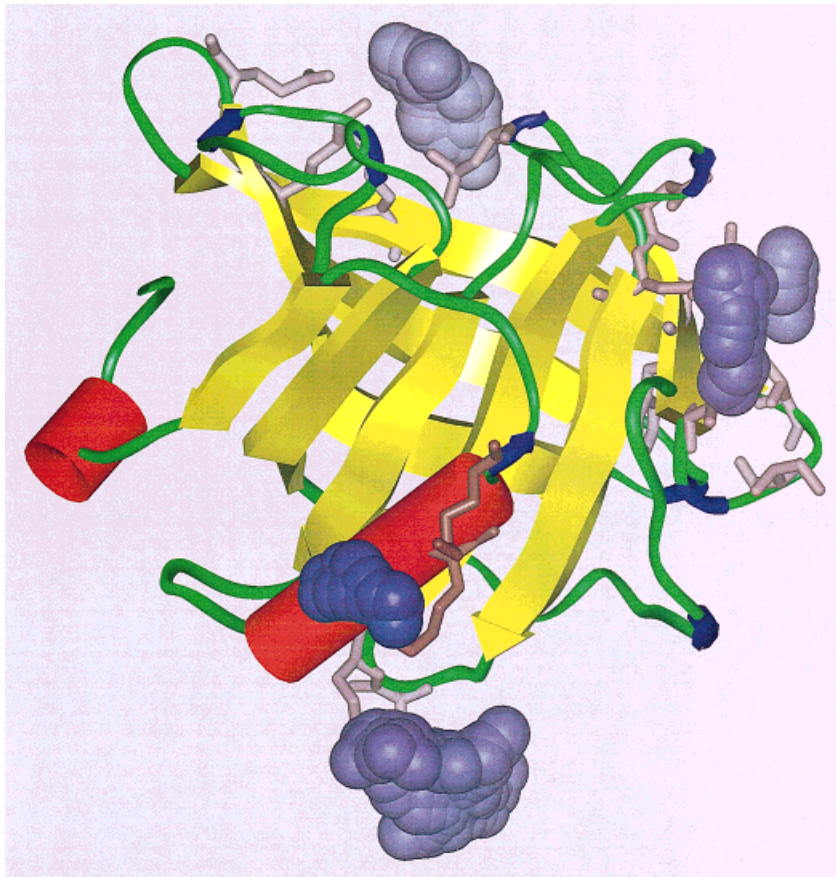

Fig. 2. Points on the surface of chain A of the dimeric form of BLG at electrostatic potential higher than ~2.5 kcal/mol · q (at low pH) shown as spheres. Bonds of contacting sidechains are shown as sticks. **Top:** The open end of the calyx. **Bottom:** Helix N-terminal and the FG loop. **Top right:** Region at the loop DE and at strands E and F.

mild changes in environmental conditions (12–120 mM ionic strength or 80–86 solvent dielectric constant to model 0 to 2 M urea concentration using linear interpolation from the dielectric constant of 95 at 5 M urea reported by Florenzano and Politi[43]) is difficult because the ionic pressure, which is neglected in our calculations and effects due to poor modelization, may be of the same order of magnitude of the differential effects we wish to compute. Both an increase in dielectric constant and in ionic strength produce changes in electrostatic forces on each atom limited in size (less than 0.1 kcal/mol · Å) similar in magnitude and direction, consistent with the similar changes in chemical shifts experimentally observed upon an increase in urea concentration or ionic strength. Atoms most largely affected in the computed electrostatic forces by the environmental changes belong prevalently to residues in high surface potential regions (e.g., Lys 60, Lys 69, Lys 91, Asp 98, Lys 101, Glu 130, Glu 131, Glu 134, Glu 135, Glu 138), in fair agreement with experimental observations (Fig. 3).

Larger effects are expected for the change in electrostatic forces upon changes in the protonation state of the molecule. As expected the largest force changes are found for residues involved in salt bridges. We report in Figure 4 the change in magnitude in the total electrostatic forces on each residue for the protonation of all acidic residues. It can be seen that three out of the twelve largest force changes are found in the terminal α-helix (Glu 134, Asp 137, Lys 138). Other residues largely affected by a decrease of pH are found in the CD loop at the open end of the calyx (Glu 62, Lys 69), in the B and C strands interface (Lys 47, Glu 55), in the FG loop (Asp 98, Lys 101), in the helix-I strand interface (Asp 137, Arg 148), and in the F and G strands interface (Lys 91, Glu 108). In Figure 5 the three regions most largely affected by changes in electrostatic forces are reported.

The onset of the change in electrostatic forces, upon decrease in pH, is triggered by protonation of acidic residues involved in the salt bridges. The pK_a has been predicted for all these residues and it has been measured for some of them via NMR. At pH 2.0 a fraction of residues Asp 28, Glu 51, Asp 53, Asp 96, Asp 98, Asp 129, Asp 130, and Asp 137 are observed to be still partly deprotonated; therefore, relevant salt bridges may still be present at low pH. It should be remembered that all these results are obtained from static structures and that the dynamic features of the protein could partly change this picture.

Protein Titration

As expected, for all molecular models the pK_a of basic sites is shifted toward more alkaline pH and the opposite effect is observed for acidic sites. However, the effect is very dependent on the structure and there are some exceptions to this general rule. The most outstanding exception is the behaviour of Glu 89 whose pK_a is shifted to 5.8/6.8 in the dimer. This residue is buried in the structure

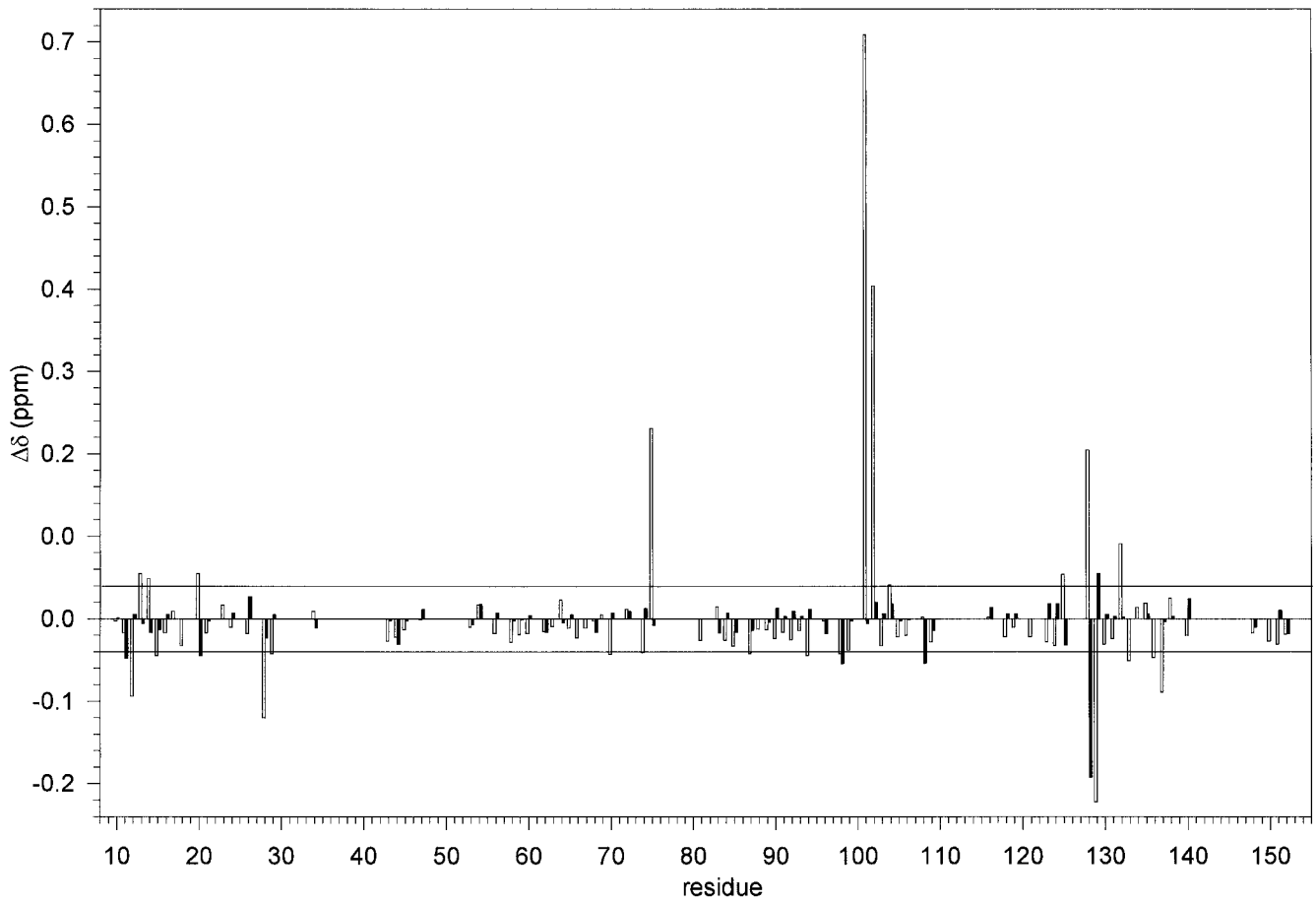

Fig. 3. Chemical shift changes upon ionic strength increase from 12 to 120 mM for HN protons (white bars) and Hα protons (black bars).

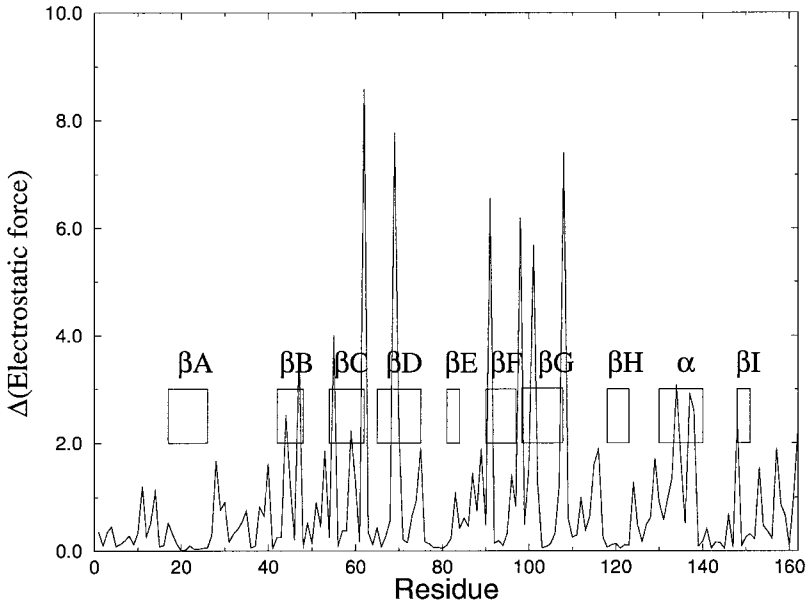

Fig. 4. Absolute change (in kcal/mol · Å) in total electrostatic forces on each residue for the protonation of all acidic residues.

and, therefore, less prone to ionization. Glu 89 is unique in showing this behaviour and, therefore, should be the anomalously titrating acidic site pointed out by Tanford and coworkers.[44] This finding is in line with the work of Brownlow and coworkers[1] who suggested Glu 89 as the anomalous titrating residue, on the basis of the X-ray

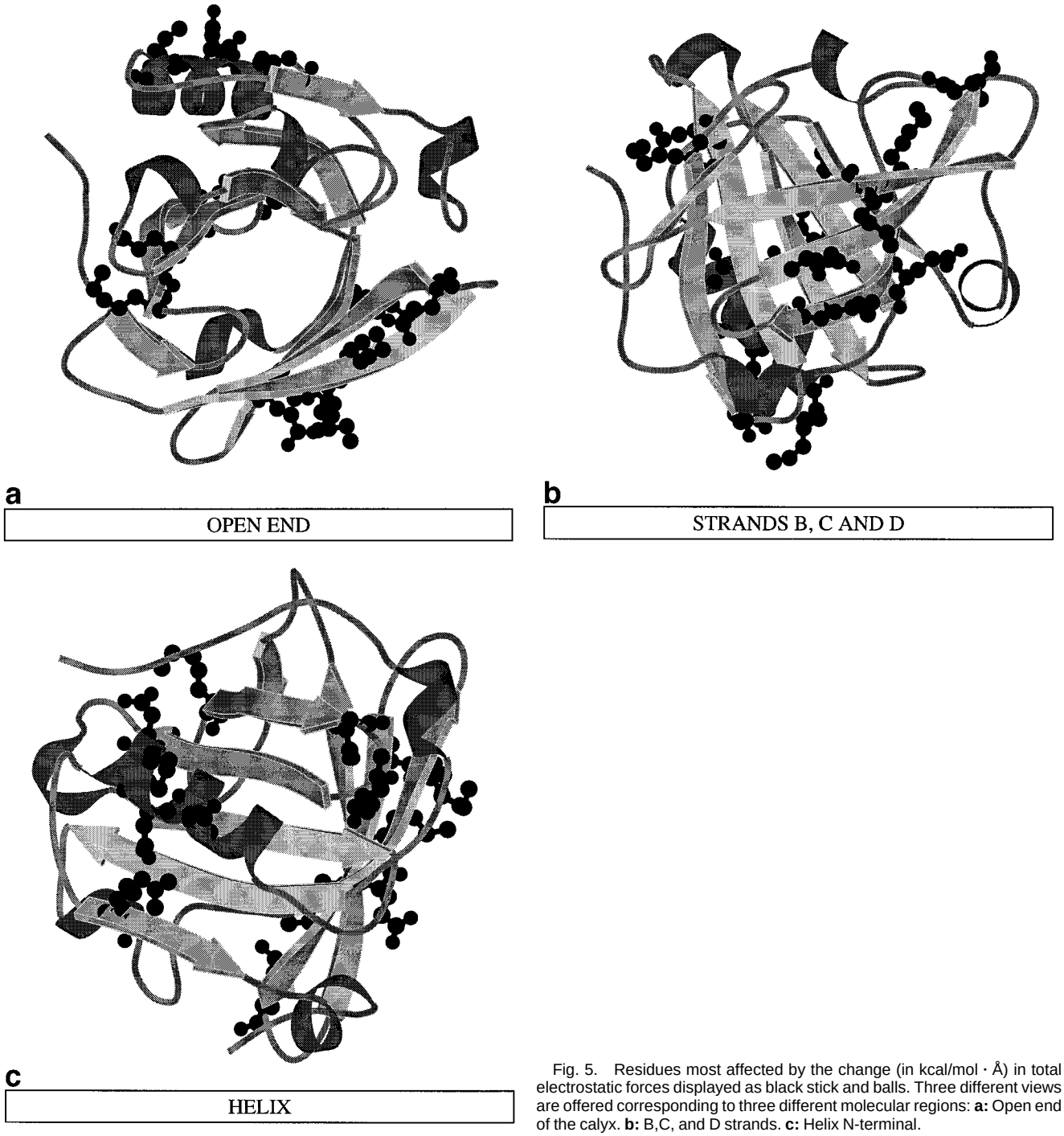

Fig. 5. Residues most affected by the change (in kcal/mol · Å) in total electrostatic forces displayed as black stick and balls. Three different views are offered corresponding to three different molecular regions: **a:** Open end of the calyx. **b:** B,C, and D strands. **c:** Helix N-terminal.

structure, and with that of Qin and coworkers who provided structural evidence for their suggestion,[2] resolving the crystal structure at three pH's close to the anomalous pK_a. The results for calculated and measured pK_a's are summarized in Tables I and II.

In most cases, pK_a's of BLG residues involved in salt bridges are more heavily shifted, consistent with what usually observed in proteins.

It is interesting to compare the results obtained on the X-ray monomeric structure artificially excised from the dimer and the ensemble of ten NMR structures. In almost all cases, pK_as are less shifted in the NMR structures, which are less compact than the X-ray one, or in other words titratable groups experience an environment closer to model compounds in the NMR structures rather than in the X-ray structure. We have computed theoretically the charge vs. pH curve and compared with the data obtained from Tanford and Nozaki[45] via potentiometric titration. We have corrected their data for the proper molecular weight of BLG, not exactly known at that time and

TABLE I. Computed and Experimental pK_as for BLG Titratable Sites for Different BLG Models

	Dimer (1beb)		Monomer (1beb)		Monomer	Monomer		
Residue	A	B	A	B	(1b0o)	(1bsq)	NMR	Experimental
Leu 1	7.9	7.9	7.7	7.8	8.3	8.5	7.4 ± 0.1	—
Lys 8	10.4	10.5	10.7	10.5	10.5	10.5	10.6 ± 0.1	—
Asp 11	2.8	2.3	2.8	2.7	2.7	3.1	3.1 ± 0.5	—
Lys 14	11.2	11.6	11.2	11.2	11.8	11.2	11.1 ± 0.5	—
Tyr 20	11.6	11.7	11.3	11.4	12.0	12.6	10.4 ± 0.3	—
Asp 28	3.5	3.1	4.1	3.8	4.5	3.4	4.0 ± 0.7	2.5 (HN, Hβ)
Asp 33	0.7	2.7	3.9	3.6	3.3	3.3	4.0 ± 0.3	—
Arg 40	19.2	17.9	15.6	15.0	17.0	18.0	13.8 ± 0.7	—
Tyr 42	14.2	13.0	13.3	12.0	10.9	11.6	11.8 ± 1.0	—
Glu 44	4.8	5.0	5.0	4.7	4.3	4.6	4.4 ± 0.2	>3.3
Glu 45	4.4	4.4	4.3	4.4	3.8	2.1	3.9 ± 0.7	>3.3
Lys 47	12.2	12.0	11.8	11.7	12.0	11.6	11.8 ± 0.3	—
Glu 51	3.9	3.9	4.2	4.1	4.3	4.6	4.4 ± 0.4	1.9–2.9 (HN, $H\beta_1$, $H\beta_2$)
Asp 53	4.0	3.6	2.2	3.5	2.5	2.5	3.4 ± 0.4	1.2–2.5 ($H\beta_1$, $H\beta_2$)
Glu 55	2.8	2.6	3.0	2.4	3.5	3.5	4.4 ± 0.4	—
Lys 60	11.0	12.3	11.1	12.1	14.1	12.8	11.6 ± 0.7	—
Glu 62	2.0	2.6	2.4	1.8	2.2	3.2	4.3 ± 0.6	>3.3
Glu 65	4.3	4.5	4.4	4.5	4.5	4.1	4.8 ± 0.4	>3.3
Lys 69	12.1	11.7	11.4	12.3	12.2	11.1	11.4 ± 0.6	—
Lys 70	11.2	11.3	11.4	11.9	11.2	11.1	11.5 ± 0.6	—
Glu 74	4.7	4.0	4.9	4.0	3.7	4.7	4.7 ± 0.4	>3.3
Lys 75	12.3	11.8	11.7	11.7	12.1	11.4	11.4 ± 0.4	—
Lys 77	10.4	9.5	10.4	9.4	10.5	10.4	10.5 ± 0.1	—
Lys 83	11.1	10.7	10.5	10.9	13.0	10.7	10.9 ± 0.4	—
Asp 85	3.5	3.8	3.6	3.8	3.8	3.8	3.8 ± 0.3	>3.3
Glu 89	5.8	6.8	6.4	5.8	4.4	4.1	4.1 ± 1.4	>3.3
Lys 91	11.6	11.0	12.3	10.9	12.2	11.0	10.9 ± 0.2	—
Asp 96	3.3	3.7	3.3	3.3	3.5	3.4	3.8 ± 0.6	1.8 (Hβ)
Asp 98	0.5	1.6	0.7	2.6	0.4	1.1	3.5 ± 0.4	2.4 (HN, Hα)
Tyr 99	11.6	10.9	11.2	10.9	10.7	11.0	9.7 ± 0.2	—
Lys 100	10.4	10.8	10.3	10.9	10.2	10.6	10.5 ± 0.5	—
Lys 101	11.3	14.1	12.0	13.3	13.5	12.6	11.5 ± 0.8	—
Tyr 102	13.9	12.9	13.1	13.3	12.7	12.5	13.0 ± 1.17	—
Glu 108	1.6	3.1	1.9	3.7	1.7	1.3	4.1 ± 0.5	—
Glu 112	4.1	4.4	4.4	3.7	3.9	4.3	4.5 ± 0.5	>3.3
Glu 114	4.0	4.1	4.0	4.0	4.6	4.3	4.8 ± 0.2	—
Cys 121	12.2	12.7	11.2	11.8	10.0	9.5	11.5 ± 0.3	—
Arg 124	15.1	14.6	14.3	14.8	15.3	15.5	13.1 ± 0.2	—
Glu 127	4.6	4.8	4.5	4.6	4.5	4.5	4.4 ± 0.2	—
Asp 129	2.4	2.3	3.1	1.7	3.1	2.4	3.9 ± 0.5	1.9–2.3 (HN, Hα)
Asp 130	3.5	3.7	3.9	4.1	4.3	4.0	3.9 ± 0.3	1.8 (Hβ)
Glu 131	4.3	1.5	4.7	2.8	4.4	4.2	4.0 ± 0.7	—
Glu 134	3.8	3.0	3.6	3.7	3.7	3.3	4.4 ± 0.3	—
Lys 135	12.2	13.1	13.5	12.9	12.0	12.1	11.8 ± 0.6	—
Asp 137	0.6	2.4	2.6	3.5	2.8	2.9	3.3 ± 0.8	2.4 (HN)
Lys 138	12.0	11.9	11.5	11.3	11.7	11.6	10.9 ± 0.2	—
Lys 141	11.5	11.1	10.7	10.6	10.6	11.2	10.7 ± 0.2	—
His 146	7.7	7.5	6.9	6.8	7.0	7.1	6.2 ± 0.7	—
Arg 148	16.2	15.2	14.4	13.5	14.9	14.2	13.6 ± 0.7	—
Glu 157	5.4	4.8	5.3	5.1	4.1	3.4	4.7 ± 0.7	—
Glu 158	4.8	4.8	4.8	4.8	5.0	4.7	4.4 ± 0.3	—
His 161	6.2	6.5	5.6	5.8	8.2	8.5	7.0 ± 0.4	—
Ile 162	3.3	3.6	2.9	3.5	3.2	3.3	3.5 ± 0.5	—

assumed to be 35,500 Da per dimer. With this correction, the charge of the monomer completely protonated, estimated from their data, is 20.6 unit charges, in outstanding agreement with the expected value of 21.0. From Figure 6 it is clearly seen that the X-ray structure obtained at higher pH does not account for the experimental data at acidic pH, which indicate a titration behaviour closer to the NMR less compact structures. A similar conclusion has been reached by Baldini et al.[46] who compared the radius of gyration of BLG at low pH, obtained by light

TABLE II. Minimum and Maximum Difference Between Experimental and Predicted pK_as for BLG Titratable Sites[†]

Residue	Prediction error [Monomer (1beb)] A	Prediction error [Monomer (1beb)] B	Prediction error (NMR)	Experimental pK_a
Asp 28	1.6	1.3	0.8–2.2	2.5 (HN, Hβ)
Glu 44	—	—	—	>3.3
Glu 45	—	—	—	>3.3
Glu 51	1.3–2.3	1.2–2.2	1.1–2.9	1.9–2.9 (HN, $H\beta_1$, $H\beta_2$)
Asp 53	−0.3–1.0	1.0–2.3	0.5–2.6	1.2–2.5 ($H\beta_1$, $H\beta_2$)
Glu 62	<−0.9	<−1.5	—	>3.3
Glu 65	—	—	—	>3.3
Glu 74	—	—	—	>3.3
Asp 85	—	—	—	>3.3
Glu 89	—	—	—	>3.3
Asp 96	1.5	1.5	1.4–2.6	1.8 (Hβ)
Asp 98	−1.7	0.2	0.7–1.5	2.4 (HN, Hα)
Glu 112	—	—	—	>3.3
Asp 129	0.8–1.2	−0.6–−0.2	1.1–2.5	1.9–2.3 (HN, Hα)
Asp 130	2.1	2.3	1.8–2.4	1.8 (Hβ)
Asp 137	0.2	1.1	0.1–1.7	2.4 (HN)

[†]For NMR structures the range of predicted pK_as is obtained by subtracting and summing one standard deviation to the average pK_a.

and X-ray scattering and the one expected from the X-ray structure.

Close to neutral pH, our theoretical model does not overlap with experimental data and the isoionic point (pH = 5.25) is underestimated by our calculations by 0.4 pH units. However, the main features of the curve are reproduced (Fig. 6). (Note that 106 titratable sites are included in the calculation and the error on the estimated charge is less than 2 unit charges per monomer).

Since the NMR structures may be artifactually less defined due to lack of experimental restraints, we have studied experimentally via NMR the titration of acidic groups between pH 1.3 and 3.3 and we compared theoretical results (on the NMR and X-ray monomeric structures) with the experimental data. A typical titration curve, which somehow illustrates the difficulties in obtaining an accurate measurement of pK_as is reported in Figure 7. The apparent agreement in the charge vs. pH plot found for the ensemble of NMR structures is partially lost when single predicted pK_as are compared with experimental data. In this respect, predictions based on the basis of the X-ray structures perform better. Beside their absolute values, the correlation with experimental data is fair in both cases. As a general remark, it is seen that carboxylic groups are not predicted to have lower pK_as than 3.1 on the basis of NMR structures. This might reflect poor modelization and absence of salt bridges for which a convenient energy term has not been taken into account in deriving the structures from NMR data. In agreement with theoretical predictions Glu 44, Glu 45, Glu 65, Glu 74, Asp 85, Glu 89, and Glu 112 do not show any appreciable change in the chemical shifts of the amide and assigned sidechain protons. Glu 62, which is predicted to titrate at 2.4–1.8 on the basis of X-ray structures and at higher pH on the basis of the NMR structures, is not seen titrating in our experimental pH range, which is consistent with the observed mobility in the CD loop.[8] There are four residues (Asp 53, Asp 98, Asp 129, Asp 137) titrating between pH 1.3 and 3.3, which are predicted to titrate on the basis of the X-ray structures and (as an average) not on the ensemble of NMR structures. Their pK_as are, however, in the lowest range predicted on the NMR ensemble of structures, with the only exception of Asp 129 for which a salt bridge with K101 is present in the X-ray structures. The low pK_a of this residue is a clear indication that a similar feature is maintained in solution at low pH.

Interesting deviations between theoretical predictions and experimental results involve Asp 28 and Asp 130, which are close (but not at) the interface between the monomers in the X-ray structure and that could be affected by rearrangements upon monomerization. For Glu 51 and Asp 96 the observed low pK_a would be consistent with formation of a salt bridge and indeed for both of them a salt bridge is detected in the X-ray structure (with Lys 75 and Lys 135, respectively). We attribute the discrepancy to details of the modeling of the contacting groups. In both cases, the low pK_a is an indication that similar structural features are preserved in solution at low pH.

The behaviour of carboxylic groups in other residues could not be observed because the corresponding peaks had not been unambigously resolved.

The apparent disagreement between the predictions of the overall charge state and the single pK_as can be explained by the fact that protons accessible by NMR are mostly found in well structured regions. These structures could be more poorly defined compared to the X-ray structures due to lack of restraints. The corresponding pK_as would then artifactually be computed closer to the unfolded residues ones. Also another possible artifact in the computation could be related to the use of a high dielectric constant to take into account partial opening dynamics, which is fully justified on a compact structure, but less on an ensemble of disordered structures. This effect is more relevant for non-exposed residues and could explain the observed differences between experimental and theoretical pK_as.

However, the overall charge state of the protein depends

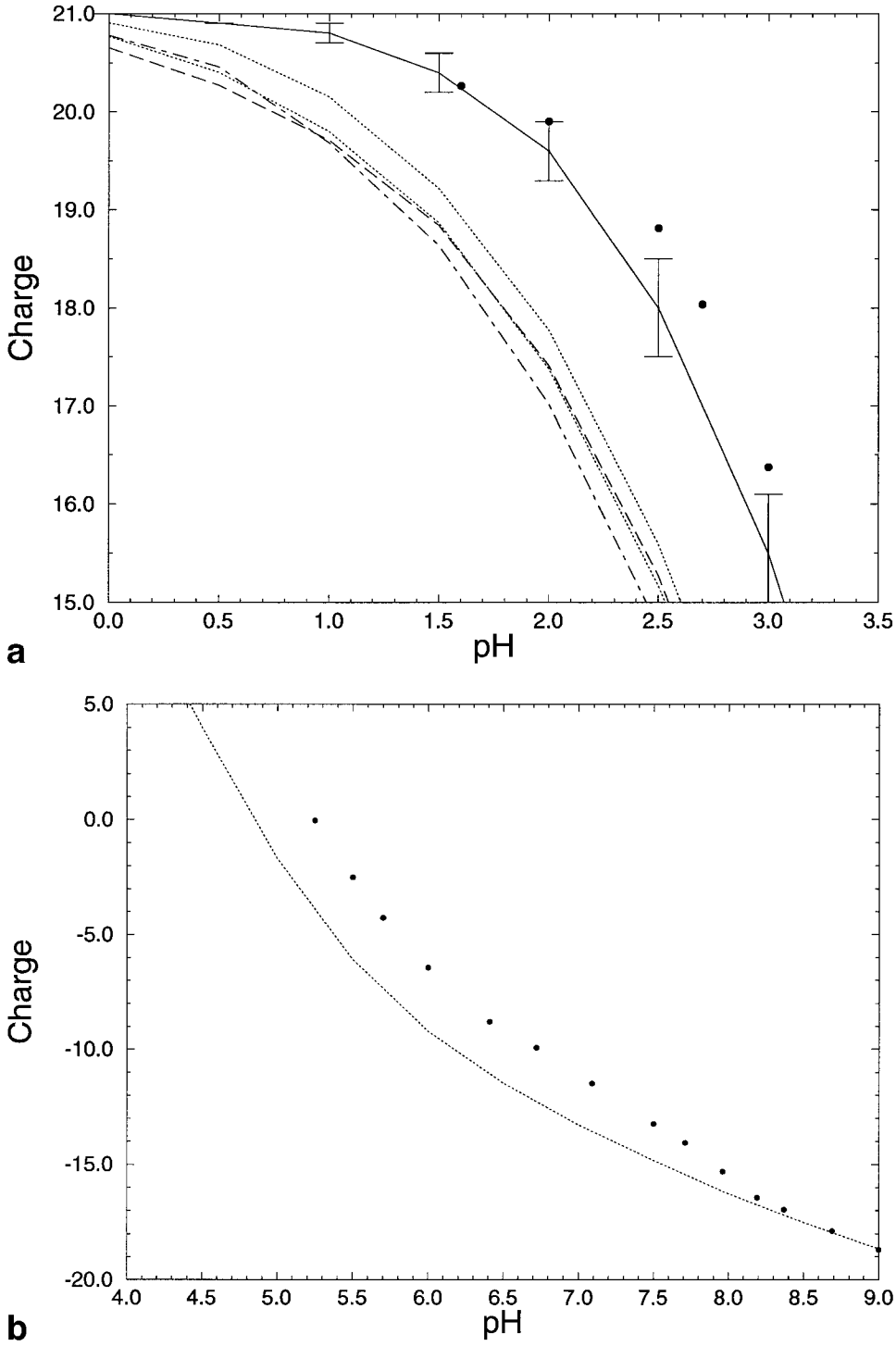

Fig. 6. **a:** Charge vs. pH for monomeric BLG at acidic pH. Experimental points obtained by Tanford and coworkers[45] are displayed as filled circles. Theoretical curves refer to: the average charge state from the ensemble of NMR structures (continuous line with error bars), BLG monomers excised from the dimer X-ray structure (PDB id.: 1beb) (dotted line), BLG monomer (variant B) at pH 7.1 from X-ray structure (PDB id.: 1bsq) (dot dashed line), BLG monomer from X-ray structure of the complex with palmitate (removed from the structure) (PDB id.: 1b0o) (dashed line). **b:** Charge vs. pH for dimeric BLG. Experimental points obtained by Tanford and coworkers[45] are displayed as filled circles. The theoretical curve has been computed for the dimer X-ray structure (PDB id.: 1beb) (dotted line).

also on residues in loops for which a compact structure (modelled in the computations by the X-ray structures) would predict overall negative shifts in pK_a larger than those corresponding to flexible regions. Thus, these results further support the picture of a protein with a core well folded and more constrained than expected from our NMR analysis, and with flexible loops and terminal regions.

CONCLUSIONS

The physico-chemical properties of BLG have been studied for a long time but its thermodynamic properties are far from being completely understood. We have investigated electrostatic properties of BLG using a methodology developed more than one decade ago but not fully explored yet. We have studied different structural models, obtained

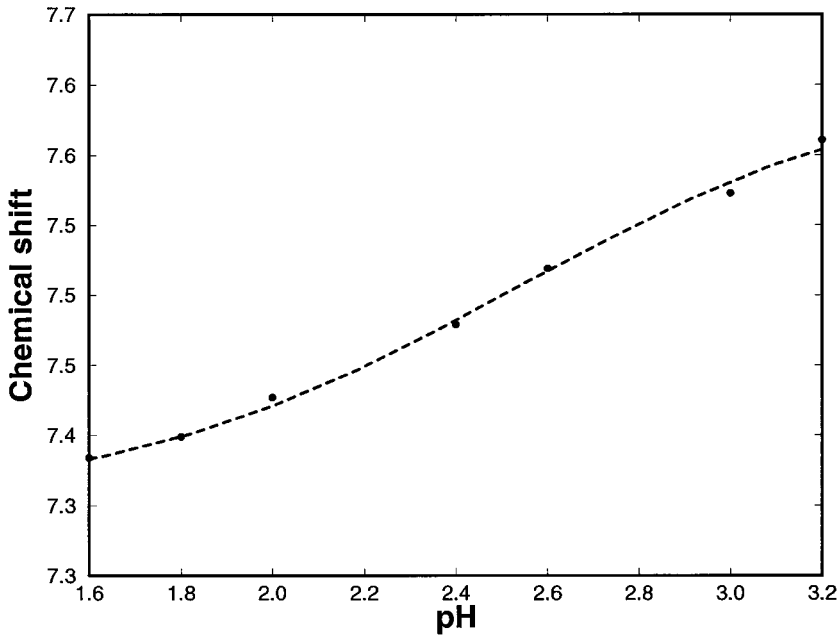

Fig. 7. Experimental titration curve for the amide proton of residue Glu 51.

from X-ray data (at physiological pH) and NMR data (at low pH). The computed changes in electrostatic forces upon changes in pH suggest that structural changes are triggered by disruption of salt bridges. Electrostatic potential pattern at the surface of the protein hint at more than one possible binding site for negatively charged ligands, like fatty acids. Theoretical predictions of titratable sites' pK_a and overall charge state at different pH's have been compared with the literature and newly obtained experimental data. The comparison suggests that even at low pH, the core of the molecule is native-like and stable, while loops and terminal regions, for which less information is available at low pH, must be disordered. The agreement between some predictions based on the X-ray structure and titration data obtained on the monomer at low pH indicates that structural features of the dimer at physiological pH are preserved on the monomers at low pH.

ACKNOWLEDGMENTS

We thank Prof J.A. McCammon for the UHBD program, Prof. B. Honig for the GRASP software, Dr. G. Vriend for the WHATIF program, and Prof. K. Wüthrich for Xeasy and Dyana programs.

REFERENCES

1. Brownlow S, Morais Cabral JH, Cooper R, Flower DR, Yewdall SJ, Polikarpov I, North ACT, Sawyer L. Bovine β-lactoglobulin at 1.8 Å resolution: still an enigmatic lipocalin. Structure 1997;5:481–495.
2. Qin BY, Bewley MC, Creamer LK, Baker HM, Baker EN, Jameson GB. Structural basis of the Tanford transition of bovine beta-lactoglobulin. Biochemistry 1998;37:14014–23
3. Qin BY, Bewley MC, Creamer LK, Baker EN, Jameson GB. Functional implications of structural differences between variants A and B of bovine β-lactoglobulin. Protein Sci 1999;8:75–83
4. Molinari H, Ragona L, Varani L, Musco G, Consonni R, Zetta L, Monaco HL. Partially folded structure of monomeric bovine β-lactoglobulin. FEBS Lett 1996;381:237–43.
5. Ragona L, Pusterla F, Zetta L, Monaco HL, Molinari H. Identification of a conserved hydrophobic cluster in partially folded β-lactoglobulin at pH 2. Fold Des 1997;2:281–290.
6. Fogolari F, Ragona L, Zetta L, Romagnoli S, De Kruif KG, Molinari H. Monomeric bovine β-lactoglobulin adopts a β-barrel fold at pH 2. FEBS Lett 1998;436:149–54.
7. Uhrinova S, Uhrin D, Denton H, Smith M, Sawyer L, Barlow PN, Complete assignment of 1H, 13C and 15N chemical shifts for bovine β-lactoglobulin: secondary structure and topology of the native state is retained in a partially unfolded form. J Biomol NMR 1998;12:89–107.
8. Ragona L, Fogolari F, Romagnoli S, Zetta L, Maubois JL, Molinari H. Unfolding and refolding of bovine β-lactoglobulin monitored by hydrogen exchange measurements. J Mol Biol 1999;293:953–969.
9. Lange DC, Kothari R, Patel RC, Patel SC. Retinol and retinoic acid bind to a surface cleft in bovine β-lactoglobulin: a method of binding site determination using fluorescence resonance energy transfer. Biophys Chem 1998;74:45–51.
10. Perez DM, Pujol P, Ena JM, Calvo M. Comparison of the ability to bind lipids of β-lactoglobulin and serum albumin of milk from ruminant and non-ruminant species. J Dairy Res 1993;60:55–63.
11. Wu S, Perez DM, Puyol P, Sawyer L. β-lactoglobulin binds palmitate within its central cavity. J Biol Chem 1999;274:170–174.
12. Davis ME, McCammon JA. Electrostatics in biomolecular structure and dynamics, Chem Rev 1990;90:509–521.
13. Honig B, Nicholls A. Classical electrostatic in biology and chemistry, Science 1995;268:1144–1149.
14. Madura JD, Davis ME, Gilson MK, Wade R, Luty BA, McCammon JA (1994). Biological applications of electrostatics calculations and Brownian dynamics simulations, Rev Comp Chem 1994;5:229–267.
15. McCammon JA, Harvey S. Dynamics of proteins and nucleic acids. Cambridge: Cambridge University Press; 1987.
16. Fogolari F, Zuccato P, Esposito G, Viglino P. Biomolecular electrostatics with the linearized Poisson-Boltzmann equation. Biophys J 1999;76:1–16.
17. Warwicker J, Watson HC. Calculation of the electric potential in the active site cleft due to alpha-helix dipoles. J Mol Biol 1982;157:671–9.
18. Gilson MK, Sharp KA, Honig B. Calculating the electrostatic potential of molecules in solution: method and error assessment. J Comp Chem 1987;9:327–335.
19. Luty BA, Davis ME, McCammon JA. Electrostatics energy calculations by a finite-difference method rapid calculations of charge-solvent interaction energies. J Comp Chem 1992;13:768–771.
20. McCoy AJ, Chandana Epa V, Colman PM. Electrostatic comple-

mentarity at protein/protein interfaces. J Mol Biol 1997;268: 570–84.
21. Verwey EJW, Overbeek ThG. Theory of the stability of lyophobic colloids. Amsterdam: Elsevier; 1948.
22. Marcus, R. A. Calculation of thermodynamic properties of polyelectrolytes. J Chem Phys 1955;23:1057–1068.
23. Zhou H-X. Macromolecular electrostatics energy within the nonlinear Poisson-Boltzmann equation. J Chem Phys 1994; 100:3152–3162.
24. Sharp KA, Honig B. Calculating total electrostatic energies with the non-linear Poisson-Boltzmann equation, J Phys Chem 1990;94: 7684–7692.
25. Fogolari F, Briggs JM. On the variational approach to the Poisson-Boltzmann free energies. Chem Phys Lett 1997;281: 135–139.
26. Sharp KA. Polyelectrolyte electrostatics: salt dependence, entropic and enthalpic contribution to free energy in the nonlinear Poisson-Boltzmann model. Biopolymers 1995;36:227–243.
27. Fogolari F, Elcock AH, Esposito G, Viglino P, Briggs JM, McCammon JA. Electrostatic effects in homeodomain-DNA interaction. J Mol Biol 1997;267:368–381.
28. Gilson MK, Davis ME, Luty BA, McCammon JA. Computation of electrostatic forces on solvated molecules using the Poisson-Boltzmann equation, J Phys Chem 1993;97:3591–3600.
29. Bashford D, Karplus M. pK_a's of ionizable groups in proteins: atomic detail from a continuum electrostatic model. Biochemistry 1990;29:10219–10225.
30. Antosiewicz J, McCammon JA, Gilson MK. Prediction of pH-dependent properties of proteins. J Mol Biol 1994;238:415–436.
31. Metropolis NA, Rosenbluth AW, Rosenbluth NM, Teller AH, Teller E. Equation of state calculation by fast computing machines. J Chem Phys 1953;21:1087–1092.
32. Madura JD, Briggs JM, Wade RC, Davis ME, Luty BA, Ilin A, Antosiewicz J, Gilson MK, Bagheri B, Scott LR, McCammon JA. Electrostatics and diffusion of molecules in solution: simulations with the University of Houston Brownian Dynamics program. Comp Phys Comm 1995;91:57–95.
33. Brooks BR, Bruccoleri RE, Olafson BD, States DJ, Swaminathan S, Karplus M. CHARMM: a program for macromolecular energy, minimization, and dynamics calculations. J Comput Chem 1983;4: 187–217.
34. MacKerell AD Jr, Bashford D, Bellott M, Dunbrack RL Jr, Evanseck JD, Field MJ, Fischer S, Gao J, Guo H, Ha S, Joseph-McCarthy D, Kuchnir L, Kuczera K, Lau FTK, Mattos C, Michnick S, Ngo T, Nguyen DT, Prodhom B, Reiher WE III, Roux B, Schlenkrich M, Smith JC, Stote R, Straub J, Watanabe M, Wiorkiewicz-Kuczera J, Yin D, Karplus M. All-atom empirical potential for molecular modeling and dynamics studies of proteins. J Phys Chem B 1998;102:3586–3616.
35. Nicholls A. GRASP: Graphical representation and analysis of surface properties. New York: Columbia University; 1993.
36. Vriend G. WHATIF: a molecular modeling and drug design program. J Mol Graphics 1990;8:52–56.
37. Demchuck E, Wade R. Improving the continuum dielectric approach to calculating pKas of ionizable groups in proteins. J Phys Chem 1996;100:17373–17387.
38. Bartels C, Xia T, Billeter M, Güntert P, Wüthrich K. The program XEASY for computer-supported NMR spectra analysis of biological macromolecules. J Biomol NMR 1995;5:1–10.
39. Qin BY, Creamer LK, Baker EN, Jameson GB. 12-Bromododecanoic acid binds inside the calyx of bovine β-lactoglobulin. FEBS Lett 1998;438:272–8.
40. Mesgarzadeh A, Pfeiffer S, Engelke J, Lassen D, Ruterjans H. Bound water in apo and holo bovine heart fatty-acid-binding protein determined by heteronuclear NMR. Eur J Biochem 1998; 251:781–786
41. Perez MD, de Villegas D, Sanchez L, Aranda P, Ena JM, Calvo M. Interaction of fatty acids with beta-lactoglobulin and albumin from ruminant milk. J Biochem 1989;106:1094–1097.
42. Hamdan M, Curcuruto O, Molinari H, Zetta L, Ragona L. Monitoring complexation between some proteins and naphtalene dye by electrospray mass spectrometry. J Mass Spect 1996;31:1261–1264.
43. Florenzano FH, Politi MJ. Effect of urea on biomimetic aggregates. Braz J Med Biol Res 1997;30:179–185.
44. Tanford C, Bunville LG, Nozaki Y. The reversible transformation of β-lactoglobulin at pH 7.5. J Am Chem Soc 1959;81:4032–4036.
45. Tanford C, Nozaki Y. Physico-chemical comparison of β-lactoglobulins A and B. J Biol Chem 1959;234:2874–2877.
46. Baldini G, Beretta S, Chirico G, Franz H, Maccioni E, Mariani P, Spinozzi F. Salt induced association of β-lactoglobulin by Light and X-ray scattering. Macromolecules 1999;32:6128–6138.